Earth and Planetary Science Letters 470 (2017) 96–107

Contents lists available at ScienceDirect

Earth and Planetary Science Letters

www.elsevier.com/locate/epsl

Effects of crustal thickness on magmatic differentiation in subduction zone volcanism: A global study

Michael J. Farner *, Cin-Ty A. Lee

Department of Earth Science, Rice University, 6100 Main Street, Houston, TX 77005, United States

ARTICLE INFO

Article history:
Received 17 October 2016
Received in revised form 3 April 2017
Accepted 13 April 2017
Available online xxxx
Editor: M. Bickle

Keywords:
magmatic differentiation
calc-alkaline
elevation
crustal thickness
Fe-depletion
arc volcanism

ABSTRACT

The majority of arc magmas are highly evolved due to differentiation within the lithosphere or crust. Some studies have suggested a relationship between crustal thickness and magmatic differentiation, but the exact nature of this relationship is unclear. Here, we examine the interplay of crustal thickness and magmatic differentiation using a global geochemical dataset compiled from active volcanic arcs and elevation as a proxy for crustal thickness. With increasing crustal thickness, average arc magma compositions become more silicic (andesitic) and enriched in incompatible elements, indicating that on average, arc magmas in thick crust are more evolved, which can be easily explained by the longer transit and cooling times of magmas traversing thick arc lithosphere and crust. As crustal thickness increases, arc magmas show higher degrees of iron depletion at a given MgO content, indicating that arc magmas saturate earlier in magnetite when traversing thick crust. This suggests that differentiation within thick crust occurs under more oxidizing conditions and that the origin of oxidation is due to intracrustal processes (contamination or recharge) or the role of thick crust in modulating melting degree in the mantle wedge. We also show that although arc magmas are on average more silicic in thick crust, the most silicic magmas (>70 wt.% SiO_2) are paradoxically found in thin crust settings, where average compositions are low in silica (basaltic). We suggest that extreme residual magmas, such as those exceeding 70 wt.% SiO_2, are preferentially extracted from shallow crustal magma bodies than from deep-seated magma bodies, the latter more commonly found in regions of thick crust. We suggest that this may be because the convective lifespan of crustal magma bodies is limited by conductive cooling through the overlying crustal lid and that magma bodies in thick crust cool more slowly than in thin crust. When the crust is thin, cooling is rapid, preventing residual magmas from being extracted; in the rare case that residual magmas can be extracted, they represent the very last melt fractions, which are highly silicic. When the crust is thick, cooling is slow, so intermediate melt fractions can readily segregate and erupt to the surface, where they cool and crystallize before highly silicic residual melts can be generated.

1. Introduction

The continental crust is enriched in silica and depleted in iron relative to a parental basaltic magma and, at least since the Proterozoic, much of it originated in subduction zone settings through arc magmatism. Melting of the mantle wedge above subducting oceanic lithosphere generates basalts, which then rise into the upper plate lithosphere where they undergo cooling and crystallization to produce evolved residual melts that go on to make the crust. Both the processes of mantle melting and intracrustal differentiation influence the compositions of arc magmas (Arndt and Goldstein, 1989; Herzberg and Rudnick, 2012; Jagoutz, 2010; Jagoutz and Schmidt, 2012; Kelemen, 1995; Lee, 2014; Lee and Bachmann, 2014; Lee et al., 2006; Plank, 2005; Plank and Langmuir, 1988; Rudnick, 1995; Turner and Langmuir, 2015a, 2015b).

A number of studies have suggested that crustal thickness plays a role in controlling the composition of arc magmas. Plank and Langmuir (1988) and Turner and Langmuir (2015a, 2015b) have shown that crustal thickness controls the composition of parental arc basalts by modulating the degree of mantle melting. Superimposed on mantle source effects are the effects of intracrustal differentiation, where fractional crystallization and other processes generate more evolved melts (Hildreth and Moorbath, 1988; Jagoutz and Schmidt, 2012; Lee and Bachmann, 2014). Progressive intracrustal differentiation eventually masks most of the

* Corresponding author.
E-mail address: mfarner01@gmail.com (M.J. Farner).

http://dx.doi.org/10.1016/j.epsl.2017.04.025
0012-821X/

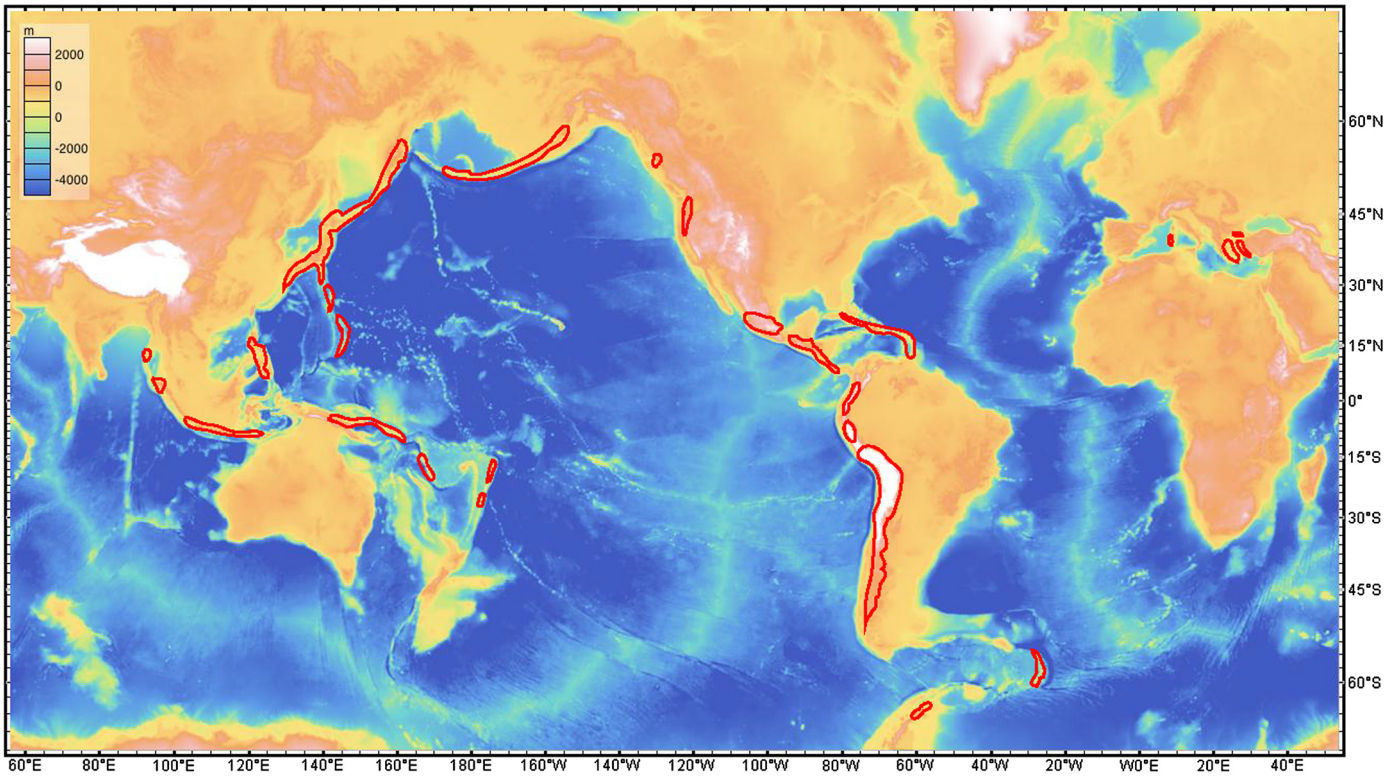

Fig. 1. Elevation (m) map of the Earth with locations of compiled arc lavas outlined in red. (For interpretation of the references to color in this figure legend, the reader is referred to the web version of this article.)

original mantle signatures, such that by the time magmas evolve to compositions typical of average continental crust, intracrustal differentiation overwhelms much of the source signal. For example, the andesitic (silicic) nature of continental crust is a result of intracrustal differentiation, and not so much due to mantle source effects, which generate basalts. Crustal thickness has also been invoked to explain the composition of more evolved arc magmas, with suggestions that thick crust favors more silicic compositions (Chapman et al., 2015; Dhuime et al., 2015; Lee et al., 2015b; Mantle and Collins, 2008).

In this paper, we explore the effects of crustal thickness on intracrustal differentiation by examining how the average composition of arc magmas varies globally with arc elevation, which we use as a proxy for crustal thickness. We find that arc magmas in thick crust have higher silica content, are more depleted in iron and more enriched in incompatible elements than magmas that traverse thin arc crust. Our observations indicate that arc magmas traversing thick crust have experienced more crystal fractionation. The greater extent of iron depletion in arc crust in thick magmatic arcs reflects earlier onset of magnetite saturation, which suggests that arc magmas traversing thick crust, such as in continental arcs, are more oxidized than arc magmas traversing thin crust, such as in island arcs. Importantly, these signatures that typify arc magmas in thick crust are the same signatures that characterize average continental crust.

2. Global arc database

We examined only Pleistocene to Holocene age volcanic rocks to insure that rock compositions reflect recent volcanism and are comparable to estimates of modern-day crustal thickness. Whole-rock compositions of lavas ($n = 52259$) were compiled from the GEOROC database (http://georoc.mpch-mainz.gwdg.de/georoc/) for all presently active volcanic arcs using precompiled data for individual arc segments (Fig. 1). Compiled data were filtered to include subaerial arc front volcanic rocks ($n = 36{,}947$) with geolocation data, a designated lithologic name (e.g. basalt, rhyolite), and major element oxide sums within the range 98–101.5 wt.% to exclude altered rocks. These data, along with meta-data, such as volcano name, magmatic arc name and coordinates, are provided in the supplemental information. Our compilation differs from other recent arc lava compilations (Plank and Langmuir, 1988; Turner and Langmuir, 2015a, 2015b), which excluded low (<4 wt.%) MgO samples for the purpose of investigating the effects of the mantle source on the compositions of primitive magmas. The objective of those studies, in particular, was to quantify the composition of primitive arc magmas by extrapolating crustal differentiation trends to a fixed MgO content (6 wt.% MgO) rather than characterizing average compositions of arc magmas "as is". In this paper, we are interested in the extent of crustal differentiation, so all magma compositions were retained to obtain an average arc magma composition. We note that the majority of arc magmas have MgO contents <6 wt.%, owing to crustal differentiation.

A number of studies have compared magma compositions with crustal thickness as constrained seismically by the depth of the Moho (Chapman et al., 2015; Hildreth and Moorbath, 1988; Mantle and Collins, 2008; Plank and Langmuir, 1988; Turner and Langmuir, 2015a, 2015b), but because seismic studies are not available everywhere, the geographic coverage of such comparisons is not comprehensive. To cover all active arcs, we assume that over long enough lengthscales, the Earth is isostatically compensated, particularly beneath active arcs where the crust is hot and weak. Lee et al. (2015b) showed that elevations of mountains correlate to first order with Moho depth (Laske et al., 2013), indicating that high elevations are isostatically compensated by crustal thickness, with mantle contributions of second order. We use the empirical correlation of elevation versus crustal thickness in Lee et al. (2015b) to convert elevation to crustal thickness and estimate lithostatic pressure at the base of the crust (assuming an average crustal density of 2870 kg/m^3).

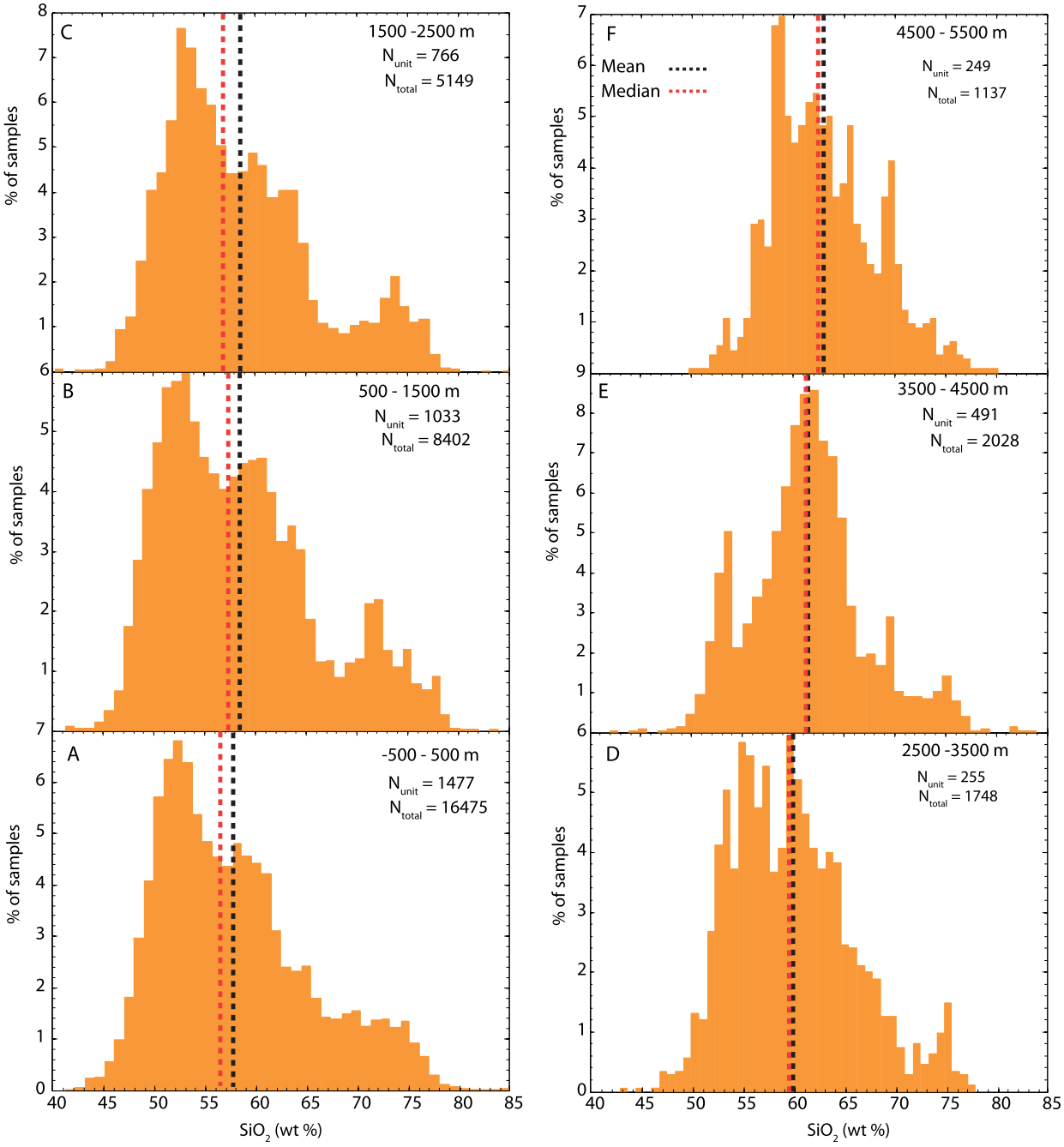

Fig. 2. (A)–(F) Normalized histograms of SiO_2 (wt.% on a volatile free basis) of compiled lavas within selected 1000 m elevation bins. Elevations are averaged over a 10 km × 10 km square horizontal area. Geochemical data are spatially averaged over unit volumes of 100 m thickness and 10 km × 10 km horizontal area ($L \times W \times h =$ 10 km × 10 km × 100 m) to suppress biases associated with oversampling of individual volcanoes. Vertical lines represent mean (black) and median (red) of unit volume averages. Total number of samples within each elevation bin is given by N_{total}. Total number of unit volumes in each 1000 m elevation bin is given by N_{unit}. (For interpretation of the references to color in this figure legend, the reader is referred to the web version of this article.)

Elevations of geo-located samples were obtained using the ESRI ArcGIS software package. Elevations for individual samples were extracted from the National Oceanographic and Atmospheric Administration ETOPO2 digital elevation model (https://www.ngdc.noaa.gov/mgg/global/etopo2) modified in ArcGIS to have a 10 km ×10 km (∼333 arcsec) horizontal grid spacing. We chose a 10 km × 10 km grid size in order to filter out non-isostatic topography, which occurs on a smaller lengthscale.

One complicating issue in data compilations is that such datasets could have sampling bias. For example, some scientifically popular volcanoes are clearly oversampled. To minimize sampling bias, we averaged compositional data over discrete volume units with horizontal dimensions of 10 km × 10 km and a vertical dimension of 100 m ($L \times W \times h =$ 10 km × 10 km × 100 m). With this approach, compositional data are spatially equal, that is, the dataset is not weighted towards any particular location. In the supplemental materials, we also present the same elevation-composition trends using data averaged over 1 km × 1 km horizontal grids (United States Geological Survey GTOPO30 digital elevation model, http://lta.cr.usgs.gov/GTOPO30/).

3. Results: elevation-composition trends

More than 83% of arc magmas in our database have MgO contents less than 6 wt.% (Fig. 2), significantly lower than primary arc basalts (>10 wt.% MgO). Thus, the great majority of arc magmas

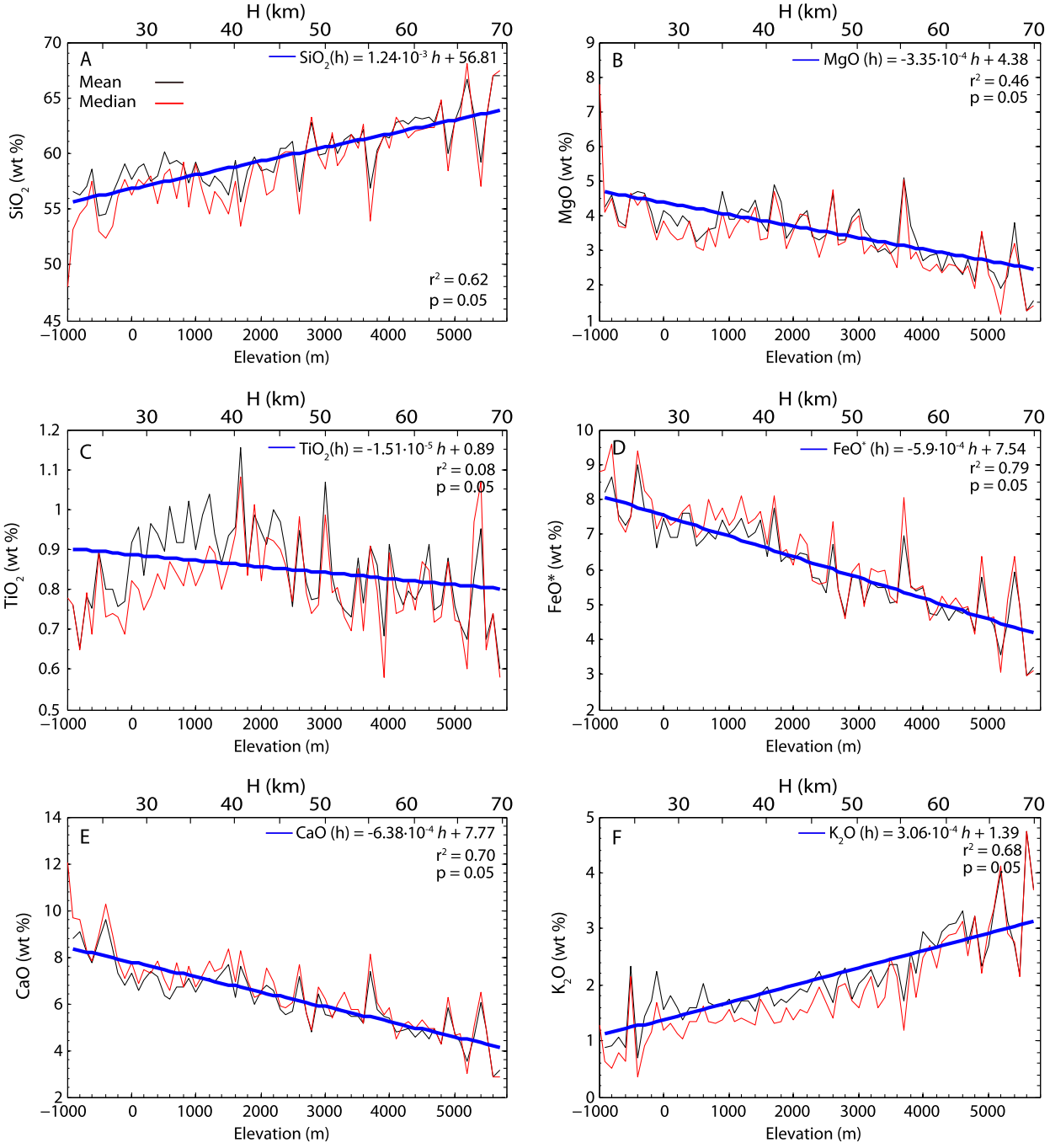

Fig. 3. (A)–(F) Mean and median major element contents of arc lavas shown as functions of elevation (averaged over 10 km × 10 km × 100 m unit volumes) with estimated crustal thickness. As elevation increases, silica (A) and potassium (F) increase while compatible major element contents (B)–(E) decrease. Equations for compositional-elevation regressions are given in supplementary materials along with calculated r^2 and p-values for the regression.

have undergone significant crystal fractionation. Systematic variations in mean and median compositions with elevation are evident when data are grouped in 100 m elevation intervals and averaged as described above. Basalt dominates at low elevations (Fig. 2A–2C) and andesite dominates at high elevations (Fig. 2D–2F) as can be seen by the increase of mean SiO_2 with increasing elevation (Fig. 3A) as well as changes in the distribution of SiO_2 with elevation. Accompanying the increase in SiO_2 with increasing elevation are increases in K_2O (Fig. 3F) and Rb/Sr (Fig. 4E), reflecting progressive enrichment in incompatible elements with elevation and silica (Figs. 3 and 4). In contrast, compatible elements like FeO* (total Fe cast as Fe^{2+}), MgO, TiO_2, and CaO, along with geochemical indices like Mg# (molar Mg/(Mg+Fe)) decrease with increasing elevation (Figs. 3B–3D and 4A–4D). We also show that elemental ratios, such as La/Yb and Gd/Yb, which are commonly attributed to garnet fractionation, increase with elevation (Figs. 5A–5B).

Recognizing that elevation correlates with crustal thickness (Lee et al., 2015b), the above observations confirm previously noted compositional relationships with crustal thickness (Chapman et al., 2015; Chiardia, 2015; Dhuime et al., 2015; Hildreth and Moorbath, 1988; Mantle and Collins, 2008; Plank and Langmuir, 1988; Turner and Langmuir, 2015a, 2015b), but our use of elevation as an indirect proxy for crustal thickness allows for more comprehensive coverage of all active arcs: from island arcs with thin crust and low elevations to continental arcs with thick crust and high elevations. Two new observations, however, are revealed as a consequence of

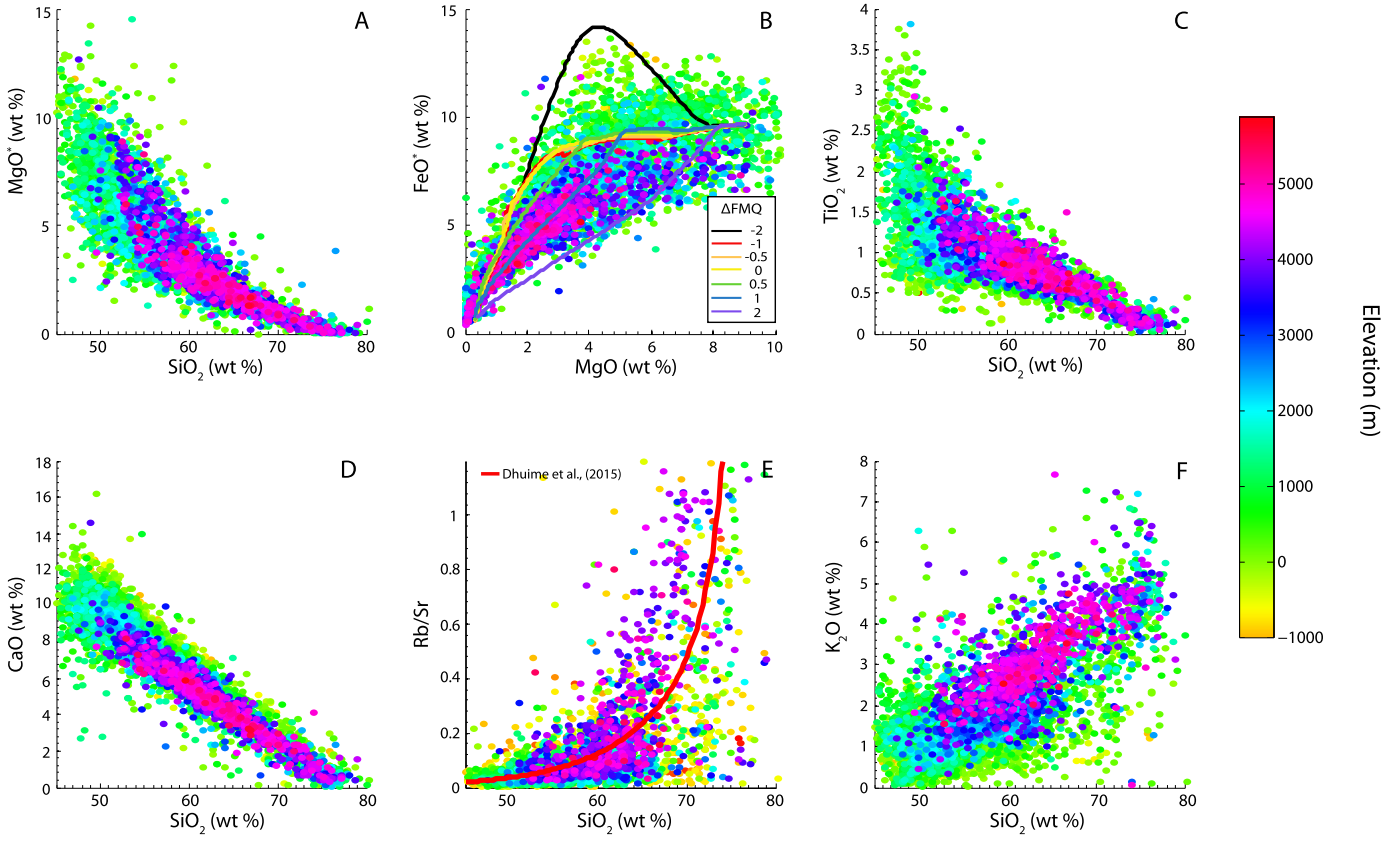

Fig. 4. (A)–(F) Variation diagrams of selected elements and elemental ratios versus SiO_2 colored by elevation. Elemental concentrations are shown for all 10 km × 10 km × 100 m unit volumes color-coded for elevation. As elevation and SiO_2 increase, compatible major element contents decrease and lavas tend toward more evolved, iron-depleted compositions. Panel B shows closed system liquid line of descent paths from a primitive hydrous (4 wt.%) basalt for different oxygen fugacities relative to the fayalite–magnetite–quartz buffer in $\log_{10}$ units (see text for details). In panel E, Rb/Sr versus SiO_2 correlation from Dhuime et al. (2015) is shown for comparison. Note that data are layered on the plot so that the highest elevation samples are in the foreground. (For interpretation of the references to color in this figure, the reader is referred to the web version of this article.)

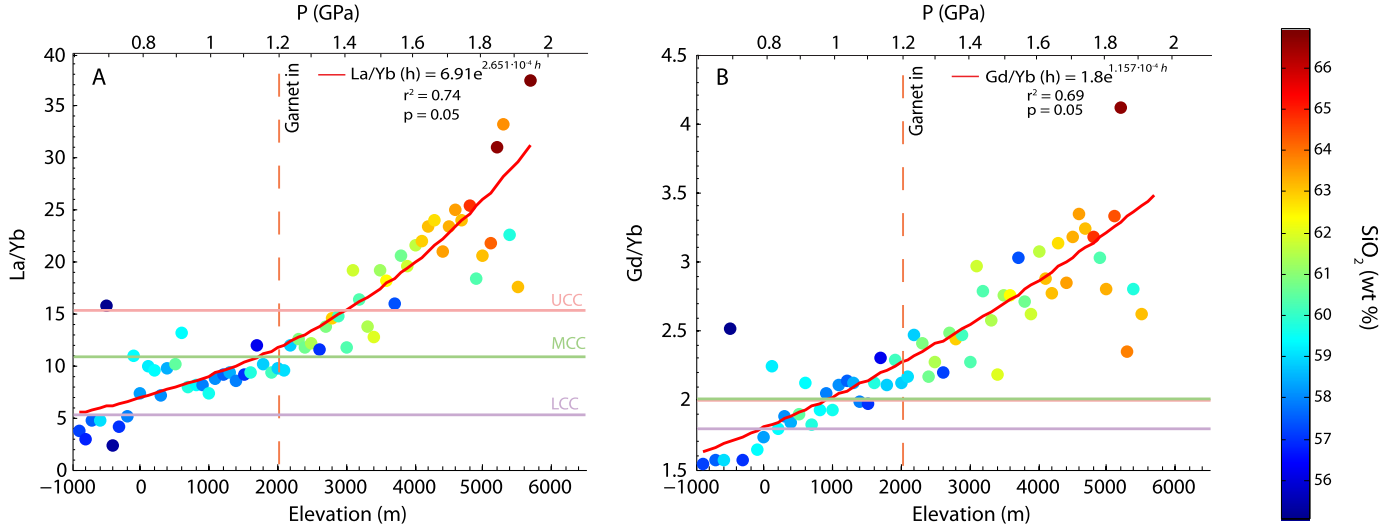

Fig. 5. (A)–(B) Global mean La/Yb and Gd/Yb, colored by average SiO_2 content, plotted against elevation and corresponding effective lithostatic pressure at the Moho as determined from inferred crustal thickness. Garnet-in pressure is from Alonso-Perez et al. (2008). UCC = upper continental crust, MCC = middle continental crust, LCC = lower continental crust from Rudnick and Gao (2003). All numbers are based on elemental concentrations averaged over 10 km × 10 km × 100 m unit volumes.

this comprehensive sampling. First, we observe systematic variations in the calc-alkaline signature of magmatic differentiation with elevation. Following Zimmer et al. (2010), the calc-alkaline signature of a magmatic differentiation series is defined by the magnitude of FeO* depletion relative to the primary magma's FeO* content. As can be seen from the global data systematics in Fig. 4B, the FeO* content of primary arc magmas does not vary significantly. For these reasons, we measure the degree of iron depletion in evolved magmas using FeO* at 5 wt.% MgO, the latter a widely used indicator of the extent of differentiation. We calculate FeO* at 5 wt.% MgO (FeO^*_{5MgO}) by averaging all samples between 4 and 6 wt.% MgO. In Fig. 6A, it can be seen that FeO^*_{5MgO} decreases

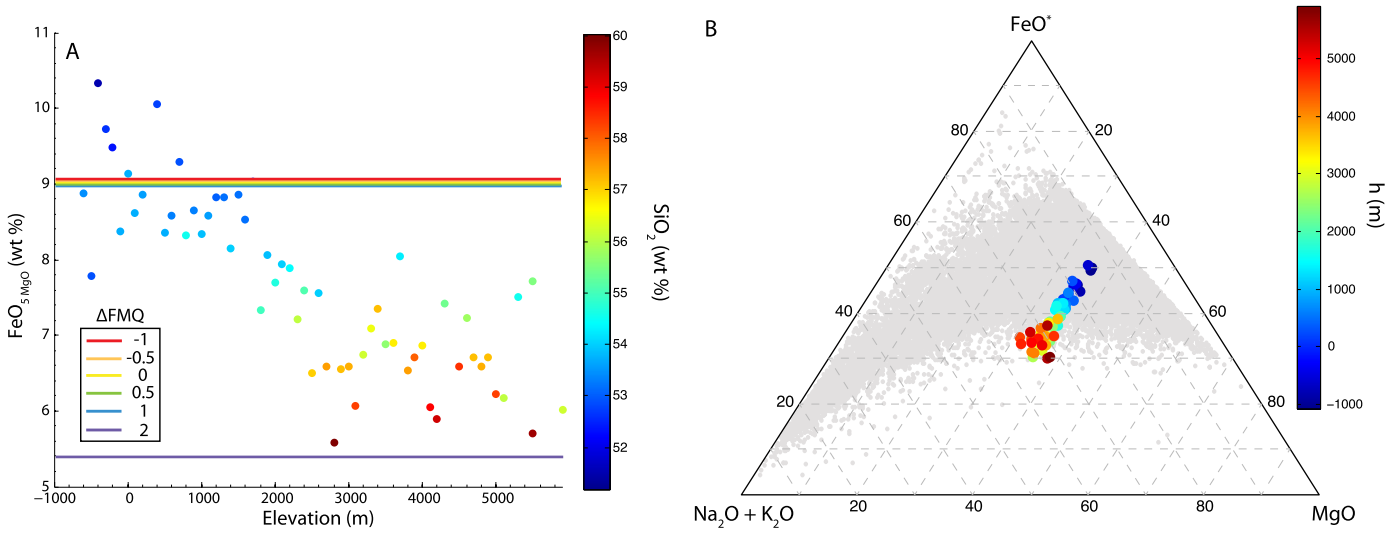

Fig. 6. (A) Global FeO^*_{5MgO} ($* =$ total Fe as FeO; 5MgO indicates FeO* is the average of all samples between 4–6 wt.% MgO) as a function of elevation, color coded for SiO_2. Oxygen fugacity contours are taken from liquid lines of descent using Rhyolite-MELTS modeling shown in Fig. 4B at MgO =5 wt.%. (B) $K_2O + Na_2O$–FeO*–MgO ternary diagram illustrating increasing calc-alkalinity with elevation (colors reflect elevation). Gray symbols represent all individual samples in the dataset. Larger symbols represent FeO^*_{5MgO} averaged over 10 km × 10 km × 100 m unit volumes. (For interpretation of the references to color in this figure, the reader is referred to the web version of this article.)

with increasing elevation, indicating that magmas, which traverse thicker crust, such as in continental arcs, differentiate along calc-alkaline paths (greater Fe depletion) whereas those that traverse thinner crust, such as in island arcs, are more tholeiitic (less Fe depletion). This can also be observed in Fig. 6B where arc lavas, on average, become more iron-depleted and alkali-enriched with increasing elevation. These observations also suggest that increasing SiO_2 content of the magma correlates with an increasing calc-alkaline signature of magma during differentiation.

The second observation is that although there is systematic variation in mean and median compositions with elevation, the difference between the mean and median decreases with increasing elevation (Fig. 3A–3F). The systematic variation in the difference between mean and median values is reflected in the symmetric frequency distributions at high elevations and skewed or even bimodal distributions at low elevations (Fig. 2A–2D), the latter due to a high silica tail that extends to rhyolitic compositions (Fig. 2E–2F). These changes in distribution apply to elevation-composition trends regardless of which digital elevation model is used (Fig. 2 and Supplementary Fig. S1), once again confirming that the trends reported here are not artifacts of the elevation model or statistical binning. Curiously, although lavas average more silicic at high elevations, the most silicic (rhyolitic) end-members are found primarily at low elevations, where basalts dominate (Fig. 2A), and are poorly represented at high elevations, where andesites dominate (Fig. 2F). It does not seem likely that this over-representation of highly silicic magmas in regions of thin crust or its under-representation in thick crust is a result of vertical sampling bias because a similar observation was reported by Lee and Morton (2015) with respect to plutonic rocks from the Cretaceous Peninsular Ranges Batholith in southern California, USA. Using heavy rare earth element systematics as a constraint on crustal thickness, they showed that plutons with andesitic compositions dominate in thick crust, but there is a paucity of highly silicic magmas (>70 wt.% SiO_2), such as granites. In thin crust, plutons average slightly less silicic than in thick crust, but the most silicic magmas in the batholith are found in thin crust. Given that both volcanic and plutonic rocks yield similar patterns in silica content distribution with crustal thickness, the observed over-representation of silicic magmas in thin crust is likely the result of magmatic processes not sampling biases.

4. Discussion

4.1. Magmatic differentiation during transport from the mantle to crustal magma reservoirs

As noted above, elevation can be translated into equivalent crustal thickness (Lee et al., 2015b), so the above compositional variations indicate variations with crustal thickness. Qualitatively, the more evolved nature of magmas with increasing crustal thickness is intuitive and unsurprising, but a more quantitative context is warranted. We begin by examining the variation of effective residual melt fraction F with crustal thickness. We can estimate the effective melt fraction F represented by an evolved magma relative to a parental basalt as the inverse of the enrichment of a highly incompatible element in the evolved magma (C) relative to that in the parental magma (C_o), that is, $F = C_o/C$. Following Lee and Morton (2015), the estimated melt fraction is independent of whether the melt represents a residual melt formed by down-temperature crystal fractionation of a basaltic magma or a derivative melt formed by up-temperature partial re-melting of a pre-existing rock, even though the physical meanings of such melts are different. The progressive increase of K_2O with increasing SiO_2 (Figs. 3F and 4F) indicates that potassium behaves perfectly incompatibly throughout magmatic differentiation, consistent with the well-known observation that K-bearing phases like biotite and alkali feldspar saturate very late in the crystallization sequence of most magmas, making it an ideal element to estimate effective melt fractions (Glazner and Johnson, 2013; Whitney, 1988).

Using an initial K_2O content (C_o) of 0.43 wt.%, determined by taking the average of the most primitive arc basalts in the dataset (MgO >12 wt.%), we can estimate how effective residual melt fraction varies as a function of crustal thickness (Fig. 7). We recognize that calculated residual F values depend on natural variations in C_o, which is controlled by the extent of melting or metasomatism in the mantle (Turner and Langmuir, 2015a, 2015b), but variations in source conditions are within a factor of 2 or 3, whereas the enrichment in highly evolved arc magmas can exceed a factor of 10, so our approach is insensitive to these uncertainties for highly evolved magmas, where extreme enrichments have been imparted by extensive crystal fractionation. As shown in Fig. 7, lavas at low elevations are represented by evolved basalts and

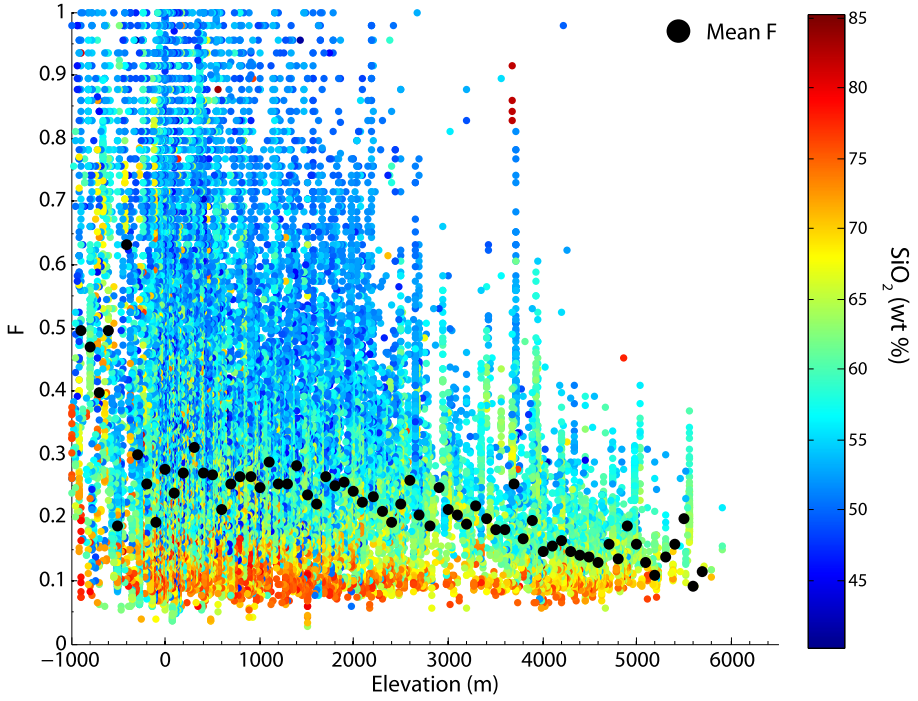

Fig. 7. Calculated effective residual melt fraction (F) as a function of elevation for all compiled data (see text for explanations). Samples are colored by SiO_2 content. Mean effective residual melt fractions for each 100 m elevation interval are shown as black circles. Residual melt fractions are calculated assuming a primitive basalt composition with 0.43 wt.% K_2O, based upon our dataset.

basaltic andesites corresponding to effective residual melt fractions of ∼30%, and at high elevations, lavas are represented by dacites corresponding to residual melt fractions of less than 20%. By comparison, rhyolitic magmas represent residual melt fractions less than 10%. If most of the observed magmatic series forms by crystal fractionation, as is widely thought, these trends imply that when magmas traverse thicker crust, they undergo more extensive crystal fractionation, generating more evolved residual magmas. While partial melting and assimilation of pre-existing crust certainly do influence magma compositions, the coherency of fractionation trends observed globally in volcanic suites indicates that crustal assimilation is likely second order compared to crystal fractionation (Jagoutz, 2010). The dominance of crystal fractionation is corroborated by nonlinear Zr and P versus SiO_2 systematics (Lee and Bachmann, 2014).

The decrease in effective residual melt fraction F with crustal thickness may not be surprising because qualitatively it would seem that the transit time of magmas migrating through thick crust might be longer than that through thin crust, allowing more time for cooling and crystal fractionation. The longer the transit time, the greater the loss of heat from the magma to the cold country rock, resulting in greater amounts of crystallization. The actual transport of magmas through the crust is undoubtedly complicated, but this concept can be illustrated with a simple model of the transit time of magma traversing the crust.

We consider melt rising through the crust in a dike cooling by conductive heat loss to the surrounding wallrock (Fig. 8A). In our simple case, we only consider the down-temperature evolution the melt with crystallization occurring on the walls of the dike and the residual melt remaining in the center of the dike. Assuming that mantle-derived magmas rise through the lithospheric mantle and crust via dikes, eventually coalescing into a crustal magma body, the transit time from the mantle to the crustal magma body is approximately L/u, where L is the distance between the Moho and the magma chamber (length of the dike) and u is the average velocity of the magma rising through the dike. Velocity is approximated by laminar channel flow driven by the intrinsic buoyancy of the magma relative to the wallrock, that is, $u \sim \Delta\rho g r^2/3\eta$, where $\Delta\rho$ is the density difference between the wallrock and melt ($\Delta\rho \sim 200$ kg/m^3), r is the radius of the dike and η is dynamic viscosity ($\eta = 100$ Pas). Crystallization extent is tracked by modeling the average temperature T_m of the magma in the ascending dike using equations given by Carslaw and Jaeger (1959) for the conductive cooling of a slab, with a constant boundary temperature representing the wallrock (T_w) of 500 °C

$$T_m(\tau) = T_w + \frac{8T_0}{\pi^2}\sum_{n=0}\frac{1}{(2n+1)^2}e^{-\kappa(2n+1)^2\pi^2\tau/4r^2} \quad (1)$$

where T_o is the initial temperature difference between the melt and wallrock temperature, κ is thermal diffusivity (10^{-6} m^2/s), r is radius of the dike and τ is the characteristic transit time ($\tau = z/u$). This constant temperature boundary condition is obviously a simplification, but we treat it as an average effective temperature.

We assume an initial melt temperature equal to the liquidus temperature of a primitive basalt from our dataset (as wt.% on a volatile-free basis, 50.74 SiO_2, 0.71 TiO_2, 16.70 Al_2O_3, 9.66 FeO*, 9.11 MgO, 10.85 CaO, 1.83 Na_2O, and 0.40 K_2O) as calculated by the Rhyolite-MELTS thermodynamic program at 0.4 GPa (Ghiorso and Gualda, 2015; Gualda et al., 2012). Using the cooling model above, we track changes in melt fraction and SiO_2 content of the cooling melt as parameterized functions of temperature based upon Rhyolite-MELTS output for closed-system crystallization such that

$$F(T) = \sum_{i=0}^{7} a_i \overline{T}^i \quad (2)$$

$$SiO_2(T) = \sum_{i=0}^{6} b_i \overline{T}^i \quad (3)$$

$$\overline{T} = \frac{T_m - T_s}{T_l - T_s} \quad (4)$$

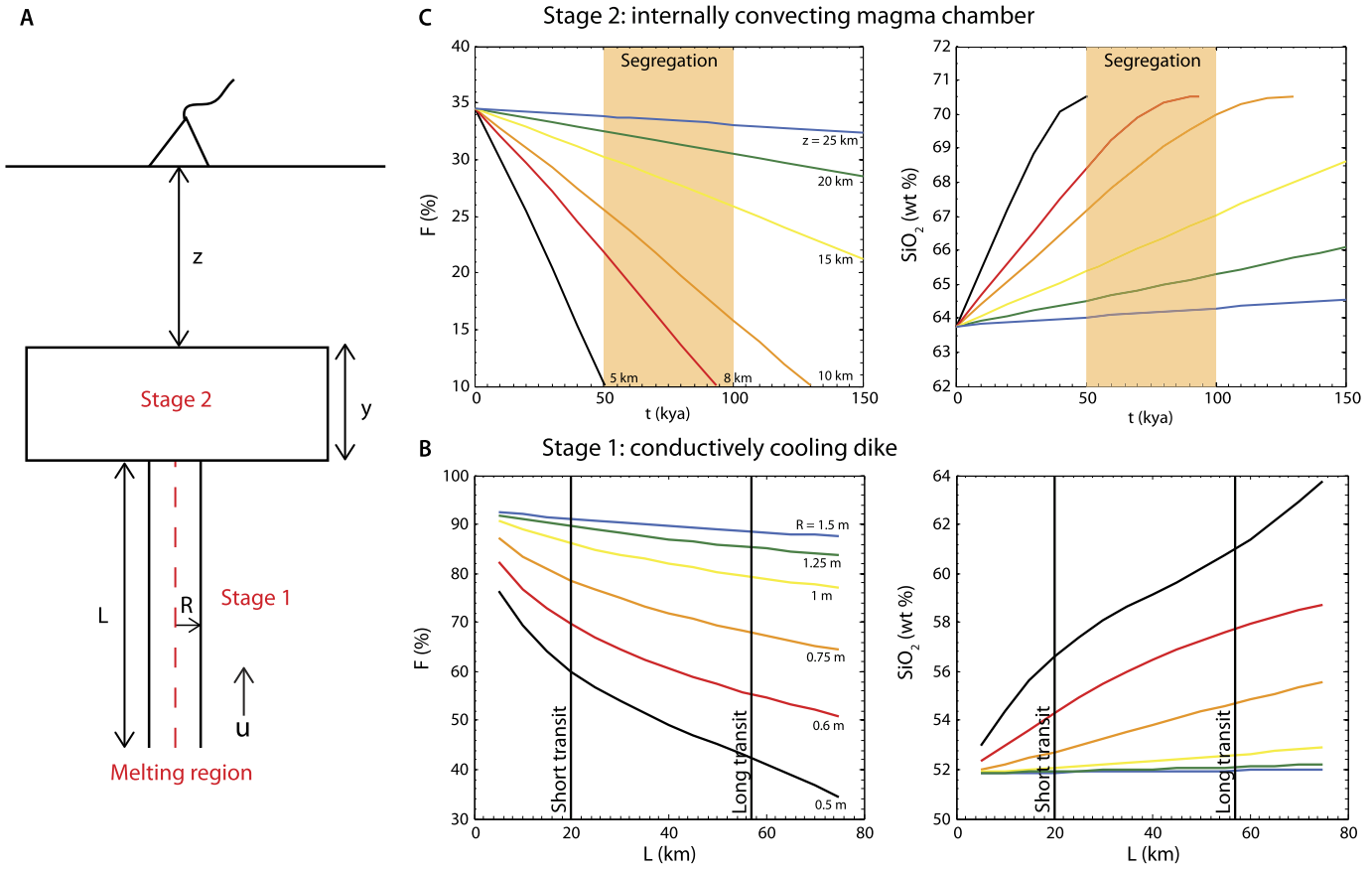

Fig. 8. Modeling the thermal and compositional evolution of a basaltic parental melt. (A) Schematic illustration of a two-stage model of melt ascent and cooling. In stage 1, the melt rises through a dike while conductively cooling. After ascending through the dike, melt ponds in a crustal magma chamber. Magma chamber (stage 2) convectively cools, but vertical heat loss out of the magma chamber is limited by conductive heat loss through the crustal lid. (B) Results for stage 1 calculations showing the effect of transit distance (L) on crystallization extent as measured by residual melt fraction F. Crystallization paths for different dike radii, which control velocity of magma ascent, are shown. Corresponding SiO_2 as a function transit distance and dike radius is also shown. (C) Model results for stage 2 calculations showing the effect of varying thickness of the crustal lid (z) on residual melt fraction F and SiO_2 content, assuming a 2 km thick magma body. It is assumed that thickness of crustal lid, that is, the depth of the magma chamber, correlates on average with crustal thickness.

where temperature $\overline{T}$ is normalized to the difference between the liquidus T_l and solidus temperatures T_s and a_i and b_i are empirical constants based upon Rhyolite-MELTS calculations for isobaric cooling of the primitive basalt composition at 0.4 GPa pressure, and oxygen fugacity fixed to the fayalite–magnetite–quartz buffer and 4 wt.% initial H_2O (Plank et al., 2013). The compositional parameters for Eqs. (2)–(4) can be found in the supplemental information. Pressure effects on these parameters play a smaller role and are not considered here.

The extent of differentiation, which scales with extent of dike cooling, depends on the effective Peclet number of the system, which is a measure of the thermal diffusion timescale relative to the dike transport timescale. Taking the thermal diffusion timescale as $t_{th} \sim r^2/\kappa$, where κ is thermal diffusivity (10^{-6} m^2/s) and the dike transport timescale is L/u, where L is the distance from the mantle to the crustal magma chamber, the expression for the Peclet number is

$$\mathrm{Pe} = \frac{\Delta\rho g r^4}{L\eta\kappa} \tag{5}$$

At high Pe, corresponding to rapid transport, long diffusive lengthscales (large r or low η) or short transit distance (L), magmas entering the crustal magma body will have only minimally cooled and differentiated and will therefore be basaltic. At low Pe numbers, corresponding to slow transport, short diffusive lengthscales, or long transit distances, magmas will have cooled and crystallized more extensively and therefore be more evolved. If transit distance L scales roughly with crustal thickness, we predict that magmas should become more evolved with increasing crustal thickness, all other variables being the same (Fig. 8B).

We recognize that the physics of this transit time model are simplified. For example, we have ignored fracture strength of the wallrock and non-buoyancy-driven overpressures that may drive magma ascent. Our approach, however, is still sufficient to show that observed variations in average silica content in island and continental arcs can, to first order, be explained by different crustal transit times. More sophisticated models are warranted, but the overall relationship between crustal thickness and extent of differentiation will not change.

4.2. Lifespan of crustal magma bodies and the composition of late segregated melts

While the average extent of fractionation can be readily explained by the transit time of magma ascent, the same model cannot explain the apparent paradox in which the most silicic magmas occur in thin crust, where lavas average basaltic (Fig. 2A). One possible explanation is that silicic magmas do not erupt to the surface in thick crust because such magmas cool, crystallize and stall during the long transit times of traversing thick crust. If this is the case, the lack of high silica rocks in regions of thick crust would be due to a bias introduced from sampling only shallowly emplaced rocks, but recent studies have shown that plutonic, which represent snapshots of magmas at depth, and volcanic rocks

are similar in bulk composition (Keller et al., 2015). Furthermore, high silica plutons are uncommon in thick crust (Lee and Morton, 2015). Thus, the lack of high silica magmas in arcs with thick crust is due to geological processes and not an artifact of vertical sampling bias. This suggests that in regions of thick crust, highly silicic melts in general are not segregated into discrete magma bodies at the surface or at depth (leucogranites are common in such environments, but they are typically of small volume), but in regions of thin crust, small amounts of silicic magmas are able to segregate while intermediate magmas are under-represented (giving a bimodal distribution of silica).

In the previous section, we examined the initial transit of melt through the crust, which we term stage 1. In this section, we consider the subsequent stage in which the accumulated intracrustal magma body cools (stage 2). In a cooling magma body, the residual melt fraction decreases and becomes more silicic with progressive cooling and crystallization. The composition of segregated melts is determined by the relative timescales of melt segregation and the thermal lifespan of the magma body, the latter defined as the time the magma body spends above the solidus. If the magma body's thermal lifespan τ_{life} is greater than the time for crystal-melt segregation τ_{seg}, melt segregation occurs before complete crystallization of the magma body, so melts of intermediate melt fraction and composition segregate. If these intermediate melt compositions erupt to the surface and quench, then highly evolved melts, like rhyolites, never have a chance to form. At the other extreme, if $\tau_{\text{life}} << \tau_{\text{seg}}$, then the magma body freezes in place before any residual melts can be expelled, so the bulk composition of this magma body will remain primitive. If $\tau_{\text{life}} \sim \tau_{\text{seg}}$, melt segregation might occur, but only late in the magma body's life, resulting in the expulsion of only low melt fraction, silicic magmas. In such a scenario, small volume silicic magma bodies, representing segregated residual liquids, should occur in the same area as more primitive, basaltic magmas, which remain compositionally similar to the parental magma.

To better quantify the above concepts, we modeled the lifespan of a crustal magma body by assuming a convecting magma body in which heat loss from the magma body is controlled by the thickness of the overlying crust, which serves as a conductive lid (Fig. 8A). Approximating the convecting magma body as well mixed and homogeneous in temperature and that the temperature gradient in the overlying conductive lid is approximately linear, the heat balance of the magma body is approximated by

$$\left(\rho c + \rho L \frac{dF}{dT}\right)\frac{dT}{dt} y = q_b - k\frac{T}{z} \tag{6}$$

where ρ is the density of the magma (crystals + melt), c is the heat capacity of the magma, L is the total latent heat, F is melt fraction, T is the temperature of the magma, y is the thickness of the magma body, z is the thickness of the overlying crustal conductive lid, and k is thermal conductivity (see supplemental data). The left-hand side represents the heat content of the magma body and includes the effect of latent heat, where dF/dT represents the efficiency of latent heat release per unit temperature change. The first term on the right-hand side represents basal mantle heat flux (q_b) into the magma body and the second term represents conductive heat loss to the surface of the Earth through the crustal lid, where surface temperature is assumed to be zero (Huber et al., 2009). Integration of this equation, valid only above the solidus, shows that the magma body cools exponentially with time

$$T = \left(T_o - \frac{q_b z}{k}\right)\exp\left(-\frac{t}{\beta z}\right) + \frac{q_b z}{k} \tag{7}$$

where T_o is the initial temperature of the magma body and $\beta = (1 + \frac{L}{c}\frac{dF}{dT})\frac{y\rho c}{k}$. The actual time τ_{life} to cool to near solidus temperatures, T_s, is then given by

$$\tau_{\text{life}} = \beta z \ln\left(\frac{T_o - q_b z/k}{T_s - q_b z/k}\right) \tag{8}$$

The characteristic timescale of cooling scales linearly with the thickness z of the overlying crustal lid. However, because the temperature of a steady state geotherm increases with depth, it takes much longer to cool a deep magma body so the *time for solidification* increases nonlinearly with depth; this can be verified by inspecting the denominator in the parenthesis term in Eq. (8). Deep crustal magma bodies thus live longer than shallow ones; for example, a 2 km thick magma body at 5 km depth freezes in ~50 ky and at 10 km depth freezes in ~150 ky (Fig. 8C).

By tracking how the composition of residual melts evolves during the cooling of the magma body (as done in the previous section), we can track how residual melt composition varies as a function of time. If melt segregation timescales are less than 50–100 ky (Cooper and Kent, 2014), it can be seen that the lifespans of magma bodies at depths greater than 10 km are longer than the segregation timescale ($\tau_{\text{life}} > \tau_{\text{seg}}$), so intermediate magmas are expelled (Fig. 8C). For magma bodies at depths of 5 km or less, $\tau_{\text{life}} < \tau_{\text{seg}}$, so magma bodies mostly freeze before any residual melts can segregate, preserving more primitive compositions. Any melts that do segregate can only be of late origin and must therefore be of low melt fraction and high silica content (Fig. 8C). Segregation of silicic liquids, driven either by hindered settling or compaction, is inefficient: segregation timescales are on the order of 10–100 ky for hindered settling and 1–100 ky for compaction, indicating that even for small volumes of silicic melt, $\tau_{\text{seg}} \sim \tau_{\text{life}}$ in thin crust and $\tau_{\text{life}} \gg \tau_{\text{seg}}$ in thick crust (Bachmann and Bergantz, 2004; Lee et al., 2015a).

If mantle-to-crust transit times (stage 1) and the depths of crustal magma bodies (stage 2) are controlled by crustal thickness, these models, despite their simplicity, can explain the distribution of silica in arc settings of different elevation and crustal thickness. As discussed above, thin crust favors less evolved, basaltic magmas, but allows for late segregation of silicic, low F residual melts, explaining why the most silicic magmas occur in thin arcs even when such arcs average basaltic. By comparison, thick crust favors intermediate magma compositions and prevents the formation of highly silicic magma bodies because melt segregation occurs well before most of the magma has crystallized and approached the highly silicic window. Instead, in thick crust, intermediate melts are segregated, which rise rapidly to the surface or erupt, freezing in the intermediate melts and never allowing an opportunity to generate highly silicic magmas.

We recognize that our two-stage model presented here is a simplification and there are many complications we have not considered. For example, growth of a thermal boundary layer within the magma body would slow cooling, while hydrothermal circulation in the upper crust would enhance cooling. We have also not considered how melt segregation rates vary as a function of cooling and melt crystallinity. However, these complicating and, in some cases, competing processes will not change the first order conclusions drawn from our simple two stage model for magmatic differentiation.

4.3. On calc-alkaline differentiation

Superimposed on the extent of magmatic differentiation are differences in the degree of iron depletion, or calc-alkalinity. As discussed above, FeO^*_{5MgO} decreases systematically as elevation increases (Fig. 6A), with arc magmas erupted through thin crust being less calc-alkaline than those erupted through thick crust. Any successful hypothesis for the origin of calc-alkaline differentiation must therefore explain why iron depletion correlates with crustal thickness and silica enrichment. One way to generate iron

depletion is by mixing mafic parental magmas with iron-poor crustal materials or evolved melts, a process that would seem more likely in thick crust (Davidson et al., 1987; Dungan et al., 2001; Hildreth and Moorbath, 1988). However, to generate large quantities of iron-depleted intermediate magmas, such as andesites, by mixing basalts and iron-poor silicic melts, such as rhyolite, requires similar proportions of rhyolite and basalt based on the fact that basalts have ~50 wt.% SiO_2, rhyolites have ~70 wt.% SiO_2 and intermediate magmas have anywhere from 60–65 wt.% SiO_2. As shown in Fig. 7, rhyolitic melts represent <10% residual melt fractions, so there is not enough rhyolitic melt formed to support the formation of intermediate magmas by mixing rhyolite with basalt.

The most popular hypothesis for iron depletion involves early saturation of magnetite, which is widely thought to be caused by high oxygen fugacities and also helps drive silica enrichment (Brounce et al., 2014; Sisson and Grove, 1993; Zimmer et al., 2010). For completeness, we have reproduced these effects of oxygen fugacity by modeling equilibrium crystallization of a primitive basalt (composition given above) with Rhyolite-MELTS using different oxygen fugacities (Fig. 4B). Melting of subarc mantle, metasomatized by oxidized fluids derived from dehydration of the subducting oceanic lithosphere, has been the dominant mechanism invoked for generating oxidized magmas (Grove et al., 2012; Kelley and Cottrell, 2009), but why oxygen fugacity and water content would be higher in arc magmas traversing thick crust is not obvious. Another possibility is that thicker crust constrains flow in the mantle wedge, decreasing the extent of mantle wedge decompression and therefore the degree of mantle melting (Karlstrom et al., 2014; Plank and Langmuir, 1988; Turner and Langmuir, 2015a, 2015b). Because hydrogen and ferric iron are highly incompatible during melting of mantle peridotite, lower degree melts of the mantle will be more oxidized and enriched in water. Consequently, mantle melts generated beneath thicker crust would tend to be more enriched in water and ferric iron, the latter manifested in melts as higher oxygen fugacity. In this "source" view, the conditions for calc-alkalinity are defined in the mantle, but controlled primarily by melting process rather than composition (Gaetani, 2016; Turner and Langmuir, 2015a, 2015b).

Magma chamber processes have also been invoked to explain the correlation of oxygen fugacity, water and crustal thickness, in part because of some suggestions that the mantle source of arc magmas is not particularly oxidized (Lee et al., 2005, 2010 2012; Mallmann and O'Neill, 2009). Specifically, deep crustal magma chambers, preceding transport to (stage 1) and storage in the middle to upper crust (stage 2) and undergoing simultaneous crystal segregation and magmatic recharge will drive incompatible components, such as water and ferric iron, to rise in concentration in the melt, beginning with only moderate amounts of these two components. However, magmatic recharge could buffer the concentrations of compatible elements, such as Mg, which, in the absence of recharge, would decrease rapidly with crystal fractionation (Lee et al., 2014; O'Neill and Jenner, 2012). Lee et al. (2014) showed that simultaneous recharge and crystallization will generate semi-primitive parental magmas with high water and ferric iron content, from which subsequent crystal fractionation proceeds along a high oxygen fugacity, calc-alkaline trend. Notably, the ferric iron content of the recharging magma need not be unusually high to begin with to generate oxidized and water-rich derivative magmas through recharge. In this view, iron oxidation state is imparted during deep intracrustal differentiation.

It is beyond the scope of this paper to further evaluate these hypotheses. What is robust is that crustal thickness modulates the onset of iron depletion. Higher oxygen fugacities are favored in arc magmas traversing thick crust, suggesting that the dynamics of melt generation or fractionation control oxygen fugacity rather than source composition.

4.4. Depth of differentiation

Finally, we note that the correlation of crustal thickness with elemental ratios such as La/Yb and Gd/Yb (Fig. 5), which indicate the involvement of garnet (a lower crustal mineral phase) during melting (Fujimaki et al., 1984; Green et al., 2000; Hauri et al., 1994; Sisson, 1994), confirms that magmas traversing thick crust undergo extensive crystal fractionation in the deep crust (Chapman et al., 2015; Chiardia, 2015). These deep crustal fractionation zones very likely occur at the base of the crust. For thin crust, La/Yb and Gd/Yb do not vary with crustal thickness, but after crustal thickness exceeds ~43 km, they begin to rise. After converting crustal thickness to pressure, we find that this critical thickness corresponds remarkably with the pressure (1.2 GPa) at which garnet first stabilizes in hydrous mafic systems (Alonso-Perez et al., 2008). The presence of garnet-bearing cumulates in deeply exposed arc sections (DeBari and Sleep, 1991; Greene et al., 2006; Jagoutz, 2010; Jagoutz et al., 2009) and of garnet-bearing cumulate xenoliths from lower arc crust and upper mantle (Chin et al., 2014; Ducea and Saleeby, 1998; Erdman et al., 2016; Esperanca et al., 1988; Lee et al., 2006) demonstrate the importance of deep crustal differentiation in controlling subsequent differentiation in the crust.

5. Conclusions and implications for continent crustal formation

We showed that the average composition of arc magmas varies with crustal thickness. On average, arc magmas are more silicic and iron-depleted in thick crust compared to thin crust. This indicates that arc magmas undergo more extensive differentiation in thick crust, which can be readily understood by the longer transit times of magmas traversing thick crust. Using coupled thermal and thermodynamic modeling, our study provides a quantitative explanation of why continental arcs are andesitic and island arcs are basaltic.

Second, we showed that the most silicic magmas in arc settings are, surprisingly, not found in thick arcs, which average more silicic than magmas in thin arcs. Instead, it is in the more basaltic, thin arcs where the most silicic magmas are found. We show that the paucity of highly silicic magmas in thick arcs and their over-representation in thin arcs may be explained by the relative timescales of magma body lifespans and crystal-melt segregation rates, the former scaling with magma chamber depth, which roughly scales with crustal thickness.

Third, we showed that the more iron-depleted nature of arc magmas traversing thick crust indicates that the onset of magnetite differentiation occurs earlier in thick crust. This observation requires that the oxidation state of iron in magmas is higher in thick arcs compared to thin arcs.

To conclude, because the average composition of the continental crust is andesitic and iron-depleted, it seems that crustal thickening, which promotes deep crustal differentiation, is a crucial step in making continental crust. This suggests that continental crust may be preferentially formed in continental arcs or during magmatic orogenic events, where thin basaltic crusts (island arcs or oceanic crust) are thickened and reprocessed.

Acknowledgements

Many thanks are due to Jean Aroom and the Rice University GIS Data Center for their help with navigating ArcGIS. We also thank Hehe Jiang, Peter Luffi, Wenrong Cao, Rajdeep Dasgupta, and Xun Yu for discussions. This work was supported by NSF grant OCE-1338842 to Lee. We thank Adam Kent, Mike Bickle and an anonymous reviewer for constructive comments.

Appendix A. Supplementary material

Supplementary material related to this article can be found online at http://dx.doi.org/10.1016/j.epsl.2017.04.025.

References

Alonso-Perez, R., Muntener, O., Ulmer, P., 2008. Igneous garnet and amphibole fractionation in the roots of island arcs: experimental constraints on andesitic melts. Contrib. Mineral. Petrol. 157, 541–558.

Arndt, N.T., Goldstein, S.L., 1989. An open boundary between lower continental crust and mantle: its role in crust formation and crustal recycling. Tectonophysics 161, 201–212.

Bachmann, O., Bergantz, G.W., 2004. On the origin of crystal-poor rhyolite: extracted from batholithic crystal mushes. J. Petrol. 45, 1565–1582.

Brounce, M.N., Kelley, K.A., Cottrell, E., 2014. Variations in $Fe^{3+}/\sum Fe$ of Mariana arc basalts and mantle wedge f_{O2}. J. Petrol. 55, 2513–2536.

Carslaw, H.S., Jaeger, J.C., 1959. Conduction of Heat in Solids. Clarendon Press, Oxford.

Chapman, J.B., Ducea, M.N., DeCelles, P.G., Profleta, L., 2015. Tracking changes in crustal thickness during Orogenic evolution with Sr/Y: an example from the North American Cordillera. Geology 43, 919–922.

Chiardia, M., 2015. Crustal thickness control on Sr/Y signatures of recent arc magmas: an Earth scale perspective. Sci. Rep. 5.

Chin, E.J., Lee, C.-T.A., Barnes, J.D., 2014. Thickening, refertilization, and the deep lithospheric filter in continental arcs: constraints from major and trace elements and oxygen isotopes. Earth Planet. Sci. Lett. 397, 184–200.

Cooper, K.M., Kent, A.J.R., 2014. Rapid remobilization of magmatic crystals kept in cold storage. Nature 506, 480–487.

Davidson, J.P., Dungan, M., Ferguson, K.M., Colucci, M.T., 1987. Crust–magma interactions and the evolution of arc magmas: the San Pedro–Pellado volcanic complex, southern Chilean Andes. Geology 15, 443–446.

DeBari, S.M., Sleep, N.H., 1991. High-Mg, low-Al bulk composition of the Talkeetna island arc, Alaska: implications for primary magmas and the nature of arc crust. Geol. Soc. Am. Bull. 103, 37–47.

Dhuime, B., Wuestefeld, A., Hawkesworth, C.J., 2015. Emergence of modern continental crust about 3 billion years ago. Nat. Geosci. 8, 552–554.

Ducea, M.N., Saleeby, J.B., 1998. The age and origin of a thick mafic-ultramafic keel from beneath the Sierra Nevada batholith. Earth Planet. Sci. Lett. 90, 26–40.

Dungan, M., Wulff, A., Thompson, R., 2001. Eruptive stratigraphy of the Tatara–San Pedro Complex, 36°S, southern volcanic zone, Chilean Andes: reconstruction method and implications for magma evolution at long-lived arc volcanic centers. J. Petrol. 42, 555–626.

Erdman, M.E., Lee, C.-T.A., Levander, A., Jiang, H., 2016. Role of arc magmatism and lower crustal foundering in controlling elevation history of the Nevadaplano and Colorado Plateau: a case study of pyroxenitic lower crust from central Arizona, USA. Earth Planet. Sci. Lett. 439, 48–57.

Esperanca, S., Carlson, R.W., Shirey, S.B., 1988. Lower crustal evolution under central Arizona: Sr, Nd and Pb isotopic and geochemical evidence from the mafic xenoliths of Camp Creek. Earth and Planetary Science Letters 90, 26–40.

Fujimaki, H., Tatsumoto, M., Aoki, K.-I., 1984. Partition coefficients of Hf, Zr and REE between phenocrysts and groundmasses. J. Geophys. Res. 89, B662–B672.

Gaetani, G.A., 2016. The behavior of $Fe^{3+}/\sum Fe$ during partial melting of spinel lherzolite. Geochim. Cosmochim. Acta 185, 64–77.

Ghiorso, M.S., Gualda, G.A.R., 2015. An H_2O–CO_2 mixing fluid saturation model compatible with rhyolite-MELTS. Contrib. Mineral. Petrol. 169, 1–30.

Glazner, A.F., Johnson, B.R., 2013. Late crystallization of K-feldspar and the paradox of megacrystic granites. Contrib. Mineral. Petrol. 166, 777–799.

Green, T.H., Blundy, J.D., Adam, J., Yaxley, G.M., 2000. SIMS determination of trace element partition coefficients between garnet, clinopyroxene and hydrous basaltic melts at 2–7.5 GPa and 1080–1200°C. Lithos 53, 165–187.

Greene, A.R., DeBari, S.M., Kelemen, P.B., Blusztajn, J., Clift, P.D., 2006. A detailed geochemical study of island arc crust: the Talkeetna arc section, south-central Alaska. J. Petrol. 47, 1051–1093.

Grove, T.L., Till, C.B., Krawczynski, M.J., 2012. The role of H_2O in subduction zone magmatism. Annu. Rev. Earth Planet. Sci. 40, 413–439.

Gualda, G.A.R., Ghiorso, M.S., Lemons, R.V., Carley, T.L., 2012. Rhyolite-MELTS: a modified calibration of MELTS optimized for silica-rich, fluid-bearing magmatic systems. J. Petrol. 53, 875–890.

Hauri, E.H., Wagner, T.P., Grove, T.L., 1994. Experimental and natural partitioning of Th, U, Pb and other trace elements between garnet, clinopyroxene and basaltic melts. Chem. Geol. 117, 149–166.

Herzberg, C., Rudnick, R.L., 2012. Formation of cratonic lithosphere: an integrated thermal and petrological model. Lithos 149, 4–15.

Hildreth, W., Moorbath, S., 1988. Crustal contributions to arc magmatism in the Andes of central Chile. Contrib. Mineral. Petrol. 98, 455–489.

Huber, C., Bachmann, O., Manga, M., 2009. Homogenization processes in silicic magma chambers by stirring and mushification (latent heat buffering). Earth Planet. Sci. Lett. 283, 38–47.

Jagoutz, O.E., 2010. Construction of the granitoid crust of an island arc, part II: a quantitative petrogenetic model. Contrib. Mineral. Petrol. 160, 359–381.

Jagoutz, O.E., Burg, J.-P., Hussain, S., Dawood, H., Pettke, T., Iizuka, T., Maruyama, S., 2009. Construction of the granitoid crust of an island arc, part I: geochronological and geochemical constraints from the plutonic Kohistan (NW Pakistan). Contrib. Mineral. Petrol. 158, 739–755.

Jagoutz, O.E., Schmidt, M.W., 2012. The formation and bulk composition of modern juvenile continental crust: the Kohistan arc. Chem. Geol. 298–299, 79–96.

Karlstrom, L., Lee, C.-T.A., Manga, M., 2014. The role of magmatically driven lithospheric thickening on arc front migration. Geochem. Geophys. Geosyst. 15, 2655–2675.

Kelemen, P.B., 1995. Genesis of high Mg # andesites and the continental crust. Contrib. Mineral. Petrol. 120, 1–19.

Keller, C.B., Schoene, B., Barboni, M., Samperton, K.M., Husson, J.M., 2015. Volcanic–plutonic parity and the differentiation of the continental crust. Nature 523.

Kelley, K.A., Cottrell, E., 2009. Water and the oxidation state of subduction zone magmas. Science 325, 605–607.

Laske, G., Masters, G., Ma, Z., Pasyanos, M., 2013. Update on CRUST1.0 – a 1-degree global model of Earth's crust. Geophys. Res. Abstr., EGU2013-2658.

Lee, C.-T.A., 2014. Physics and chemistry of deep continental crust recycling. In: Holland, H., Turekian, K. (Eds.), Treatise of Geochemistry, 2nd ed. Elsevier, pp. 423–456.

Lee, C.-T.A., Bachmann, O., 2014. How important is the role of crystal fractionation in making intermediate magmas? Insights from Zr and P systematics. Earth Planet. Sci. Lett. 393, 266–274.

Lee, C.-T.A., Cheng, X., Horodyskyj, U., 2006. The development and refinement of continental arcs by primary basaltic magmatism, garnet pyroxenite accumulation, basaltic recharge and delamination: insights from the Sierra Nevada, California. Contrib. Mineral. Petrol. 151, 222–242.

Lee, C.-T.A., Lee, T.C., Wu, C.-T., 2014. Modeling the compositional evolution of recharging, evacuating, and fractionating (REFC) magma chambers: implications for differentiation of arc magmas. Geochim. Cosmochim. Acta 143, 8–22.

Lee, C.-T.A., Leeman, W.P., Canil, D., Li, Z.-X.A., 2005. Similar V/Sc systematics in MORB and arc basalts: implications for the oxygen fugacities of their mantle source regions. J. Petrol. 46, 2313–2336.

Lee, C.-T.A., Luffi, P., Chin, E.J., Bouchet, R., Dasgupta, R., Morton, D.M., Le Roux, V., Yin, Q.-z., Jin, D., 2012. Copper systematics in arc magmas and implications for crust–mantle differentiation. Science 336, 64–68.

Lee, C.-T.A., Luffi, P., Le Roux, V., Dasgupta, R., Albarède, F., Leeman, W.P., 2010. The redox state of arc mantle using Zn/Fe systematics. Nature 468, 681–685.

Lee, C.-T.A., Morton, D.M., 2015. High silica granites: terminal porosity and crystal settling in shallow magma chambers. Earth Planet. Sci. Lett. 409, 23–31.

Lee, C.-T.A., Morton, D.M., Farner, M.J., Moitra, P., 2015a. Field and model constraints on silicic melt segregation by compaction/hindered settling: the role of water and its effect on latent heat release. Am. Mineral. 100, 1762–1777.

Lee, C.-T.A., Thurner, S., Paterson, S., Cao, W., 2015b. The rise and fall of continental arcs: interplays between magmatism, uplift, weathering, and climate. Earth Planet. Sci. Lett. 425, 105–119.

Mallmann, G., O'Neill, H.S.C., 2009. The crystal/melt partitioning of V during mantle melting as a function of oxygen fugacity compared with some other elements (Al, P, Ca, Sc, Ti, Cr, Fe, Ga, Y, Zr and Nb). J. Petrol. 50, 1765–1794.

Mantle, G.W., Collins, W.J., 2008. Quantifying crystal thickness variations in evolving orogens: correlation between arc basalt compositions and Moho depth. Geology 36, 87–90.

O'Neill, H.S.C., Jenner, F.E., 2012. The global pattern of trace element distributions in ocean floor basalts. Nature 491, 698–705.

Plank, T., 2005. Constraints from Thorium/Lanthanum on sediment recycling at subduction zones and the evolution of the continents. J. Petrol. 46, 921–944.

Plank, T., Kelley, K.A., Zimmer, M.M., Hauri, E.H., Wallace, P.J., 2013. Why do mafic arc magmas contain ~4 wt.% water on average? Earth Planet. Sci. Lett. 364, 168–179.

Plank, T., Langmuir, C.H., 1988. An evaluation of the global variations in the major element chemistry of arc basalts. Earth Planet. Sci. Lett. 90, 349–370.

Rudnick, R.L., 1995. Making continental crust. Nature 378, 571–578.

Rudnick, R.L., Gao, S., 2003. Composition of the continental crust. In: Holland, H.D., Turekian, K.K. (Eds.), Treatise on Geochemistry. Elsevier-Pergamon, Oxford, pp. 1–64.

Sisson, T.W., 1994. Hornblende-melts trace element partitioning measured by ion microprobe. Chem. Geol. 117, 331–344.

Sisson, T.W., Grove, T.L., 1993. Experimental investigations of the role of H_2O in calc-alkaline differentiation and subduction zone magmatism. Contrib. Mineral. Petrol. 113, 143–166.

Turner, S.J., Langmuir, C.H., 2015a. The global chemical systematics of arc front stratovolcanoes: evaluating the role of crustal processes. Earth Planet. Sci. Lett. 422, 182–193.

Turner, S.J., Langmuir, C.H., 2015b. What processes control the chemical composition of arc front stratovolcanoes? Geochem. Geophys. Geosyst. 16, 1865–1893.
Whitney, J.A., 1988. The origin of granite: the role and source of water in the evolution of granitic magmas. Geol. Soc. Am. Bull. 100, 1886–1897.
Zimmer, M.M., Plank, T., Hauri, E.H., Yogodzinski, G.M., Stelling, P., Larsen, J., Singer, B., Jicha, B., Mandeville, C., Nye, C.J., 2010. The role of water in generating the calc-alkaline trend: new volatile data for Aleutian magmas and new tholeiitic index. J. Petrol. 51, 2411–2444.